



## Effect of fiber arrangement on mechanical properties of short fiber reinforced composites

H.F. Lei<sup>a</sup>, Z.Q. Zhang<sup>b,\*</sup>, B. Liu<sup>a,c,\*</sup>

<sup>a</sup> AML, Department of Engineering Mechanics, Tsinghua University, Beijing 100084, China

<sup>b</sup> Department of Engineering Mechanics, Institute of High Performance Computing, 138632 Singapore, Singapore

<sup>c</sup> Department of Engineering Mechanics, Tsinghua University, Beijing 100084, China

### ARTICLE INFO

#### Article history:

Received 16 June 2011

Received in revised form 9 November 2011

Accepted 11 December 2011

Available online 17 December 2011

#### Keywords:

A. Short-fiber composites

B. Mechanical properties

Biomimetic composites

### ABSTRACT

The present paper developed a three-dimensional (3D) “tension–shear chain” theoretical model to predict the mechanical properties of unidirectional short fiber reinforced composites, and especially to investigate the distribution effect of short fibers. The accuracy of its predictions on effective modulus, strength, failure strain and energy storage capacity of composites with different distributions of fibers are validated by simulations of finite element method (FEM). It is found that besides the volume fraction, shape, and orientation of the reinforcements, the distribution of fibers also plays a significant role in the mechanical properties of unidirectional composites. Two stiffness distribution factors and two strength distribution factors are identified to completely characterize this influence. It is also noted that stairwise staggering (including regular staggering), which is adopted by the nature, could achieve overall excellent performance. The proposed 3D tension–shear chain model may provide guidance to the design of short fiber reinforced composites.

© 2011 Elsevier Ltd. All rights reserved.

## 1. Introduction

Biological materials such as bone and nacre are made of mineral and protein. While the mineral is as stiff as chalk with relatively low fracture toughness and the protein is as compliant as skin with relatively high ductility, many studies [1–3] have indicated that the stiffness and toughness of these biocomposites are comparable to their stiff and tough constituents, respectively. Further studies [1,2,4–8] found that these biological materials have very similar nano-structures: the hard platelets or fibers are staggered within the soft matrix, as shown in Fig. 1. These structures are considered as crux [9–11] of the superior mechanical properties of the biological materials.

Several studies on biocomposites with staggered platelets have been conducted. Jager and Fratzl [11] proposed a model with staggered array of platelets, which successfully reproduced the fact that both the elastic modulus and rupture stress are increased with the amount of mineral. Ji and Gao [12] assumed the load in the longitudinal direction is mainly transferred via shear in matrix and developed a tension–shear chain model, for regular staggering situation (platelets overlap with half of their length) to illustrate how

biocomposites achieve high stiffness and toughness, which can be used to interpret many mechanisms of the behaviors of biocomposites. Nonetheless, there also exist some distributions of reinforcement phase other than regular staggering, such as the stairwise staggering of bone shown in Fig. 1b. Moreover, with the progress of micro/nano-scale manipulation, Tang et al. [13] and Bonderer et al. [14] successfully fabricated biomimetic materials with non-uniform or even random platelets alignment. The studies of Zhang et al. [15] further developed the tension–shear chain model by investigating the effect of arbitrary distributions of reinforced platelets on the mechanical properties of biocomposites.

On the other hand, short fiber reinforced composites have been widely used and studied for a long time [16–19,31,32]. Especially in recent years, carbon nanotube is considered to be an ideal reinforcement phase [20–29] for new generation of high-performance composites. Similar to platelet reinforced composites stated above, introducing bio-inspired alignment of reinforcements into short fiber reinforced composites is also expected to produce better mechanical properties. Zhang and Liu [30] extended the tension–shear chain model to predict the axial Young's modulus of bio-mimetic composites with discontinuous fibers aligned in a regularly staggered pattern. However, the cases with other staggered patterns have not been systematically studied.

The purpose of this paper is to investigate the effects of non-uniform or random distribution of unidirectional short fibers on the mechanical properties of composites through a theoretical

\* Corresponding authors. Address: AML, Department of Engineering Mechanics, Tsinghua University, Beijing 100084, China (B. Liu).

E-mail addresses: [zhangqz@ihpc.a-star.edu.sg](mailto:zhangqz@ihpc.a-star.edu.sg) (Z.Q. Zhang), [liubin@tsinghua.edu.cn](mailto:liubin@tsinghua.edu.cn) (B. Liu).

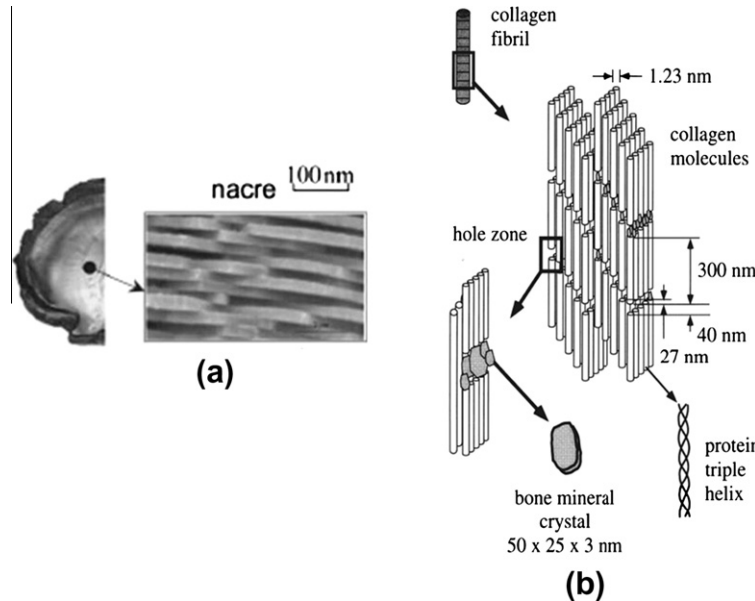


**Fig. 1.** Nanostructures of (a) nacre (Reprinted with permission from [9]) and (b) bone (Reprinted with permission from [8]).

model and FEM calculations. The paper is outlined as follows. In Section 2, the analytical model for short fiber reinforced composites is developed, and corresponding FEM model is also presented. The effects of various parameters, especially fiber distribution, on the mechanical properties of composites are investigated in Section 3. Main conclusions are summarized in Section 4.

## 2. Analytical and FEM model for short fiber reinforced composites

This paper is focused on studying the effective mechanical properties of composites consisting of stiff short-fibers unidirectionally distributed in the soft matrix. For simplicity, it is assumed that all fibers have the same length  $L$  and radius  $R$ , transversely distributed in a triangle lattice pattern with transverse spacing  $d$ , as shown in Fig. 2, and thus the periodicity is always guaranteed in the longitudinal direction ( $z$  direction). A representative unit cell of the composites shown in Fig. 2 has  $m$  rows and  $n$  columns of fibers, so there are  $s = m \times n$  fibers in a unit cell. Denote the longitude position of the  $i$ th fiber in Fig. 2b as  $z = \xi_i L$  ( $0 \leq \xi_i < 1$ ,  $i = 1, 2, \dots, s$ ) in the global coordinate. When we study the interaction of  $i$ th fiber and its neighbors, a local coordinate  $\tilde{z} = z - \xi_i L$  is introduced, thus  $\tilde{z} = 0$  for the  $i$ th fiber and  $\tilde{z} = \xi_j L$  for its neighboring fibers. Briefly,  $\xi_i$  denotes the normalized coordinate of the  $i$ th fiber in the global coordinate system while  $\xi_{ij}$  is the normalized coordinate of the  $j$ th fiber in the local coordinate system related to the subset of the  $i$ th fiber and it is completely determined by  $\xi_i$  and  $\xi_j$ :

$$\xi_{ij} = \begin{cases} \xi_j - \xi_i, & \text{if } \xi_j \geq \xi_i \\ \xi_j - \xi_i + 1, & \text{if } \xi_j < \xi_i \end{cases} \quad (1)$$

### 2.1. Three dimensional tension-shear chain model

To obtain simple analytical formulae, a 3D tension-shear chain model is developed under the following assumptions:

- (1) The gap between the fibers is much smaller than their length and can be ignored.
- (2) The diameter of fibers is one or two orders of magnitude smaller than their length, thus the deformation of the fibers can be considered as one dimensional (only depends on  $z$ ).

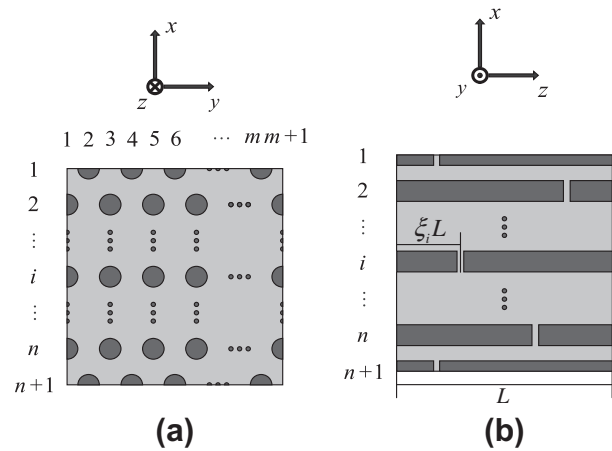


**Fig. 2.** Schematic of unidirectional short-fibers reinforced composites: (a) cross section view of a unit cell, (b) side view of a unit cell.

- (3) The modulus of fibers is much larger than that of the matrix (at least two to three orders of magnitude), and thus the normal stress of the matrix can be ignored.
- (4) Both of the fibers and matrix are assumed to be linear elasticity until failure.
- (5) A piecewise uniform distribution along  $z$  is assumed for the shear stress field in the matrix between two neighboring fibers, and thus a piecewise linear profile for the normal stress in each fiber.

Note that the assumption of (5) has been shown valid for most biological and biomimetic materials by Liu et al. [33], and is also verified in this paper through comparing our theoretical predictions and FEM results. More important, the uniform shear stress assumption makes it possible for us to derive the explicit solutions of effective Young's modulus, strength, failure strain and energy storage capacity for various distributions with avoiding such complicate mathematics as occurs in elastic shear-lag theory.

Based on the above assumptions, we divide the matrix of fibers reinforced composites into two regions, the shear region and the

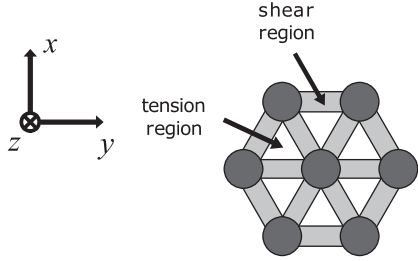


Fig. 3. Cross section view of the shear region and tension region of matrix.

tension region, as shown in Fig. 3. The tension region of the matrix mainly bears normal stress, while the shear region of the matrix transfers the load between the neighboring fibers via shear. Furthermore, according to the assumption (3), we can regard that the normal stress is fully undertaken by the fibers and neglect the contribution of the tension region of the matrix.

Take out the  $i$ th fiber and its neighbor, the  $j$ th fiber, to analyze the transfer of stress between neighboring fibers in the composite, as shown in Fig. 4. Combined the assumptions (4) and (5), we can obtain the following relations:

$$\gamma_{ij}^U(\theta) = \frac{w_{ij}^U}{d + 2R - 2R\cos\theta}, \quad (2)$$

$$\tau_{ij}^U(\theta) = G_m \gamma_{ij}^U(\theta), \quad (3)$$

where  $\gamma_{ij}^U$  and  $\tau_{ij}^U$  are the  $yz$  components of shear strain and stress in the upper shear region, respectively, and both of them are just functions of  $\theta$  (see Fig. 4a);  $w_{ij}^U$  is a constant for this shear region, which can be seen as the rigid displacement of the upper part of the  $j$ th fibers relative to the  $i$ th fiber (as shown in Fig. 4b);  $G_m$  is the shear modulus of the matrix.

The shear force per unit length  $T_{ij}^U$  along  $z$ -direction generated by the upper part of the  $j$ th fiber can be obtained by integrating over the arc

$$T_{ij}^U = \int_{-\frac{\pi}{6}}^{\frac{\pi}{6}} \tau_{ij}^U(\theta) R \cos \theta d\theta = C_0 G_m w_{ij}^U, \quad (4)$$

where

$$C_0 = \left[ \frac{2R + d}{\sqrt{d(d + 4R)}} \arctan \left( \sqrt{\frac{d + 4R}{d}} \tan \left( \frac{\theta}{2} \right) \right) - \frac{\theta}{2} \right] \Big|_{-\frac{\pi}{6}}^{\frac{\pi}{6}} \quad (5)$$

is a constant derived by the integration in Eq. (4) combined with Eqs. (2) and (3).

Combining Eqs. (2)–(4), the relationship of the shear stress  $\tau_{ij}^U$  and shear force per unit length  $T_{ij}^U$  can be acquired

$$\tau_{ij}^U(\theta) = \frac{T_{ij}^U}{C_0(d + 2R - 2R\cos\theta)}. \quad (6)$$

Applying the similar analysis to the lower part of the  $j$ th fiber, the full field of shear stress between the  $i$ th and  $j$ th fiber can be got as follows:

$$\begin{cases} \tau_{ij}^L(\theta) = \frac{T_{ij}^L}{C_0(d + 2R - 2R\cos\theta)}, & \tilde{z} < \tilde{\xi}_{ij}L \\ \tau_{ij}^U(\theta) = \frac{T_{ij}^U}{C_0(d + 2R - 2R\cos\theta)}, & \tilde{z} \geq \tilde{\xi}_{ij}L \end{cases}. \quad (7)$$

Based on the geometrical relationship, the volume fraction of fibers in the composite is  $\Phi = 2\pi R^2 / [\sqrt{3}(d + 2R)^2]$ . And, another configuration parameter, the aspect ratio of fibers, is  $\rho = L/(2R)$ .

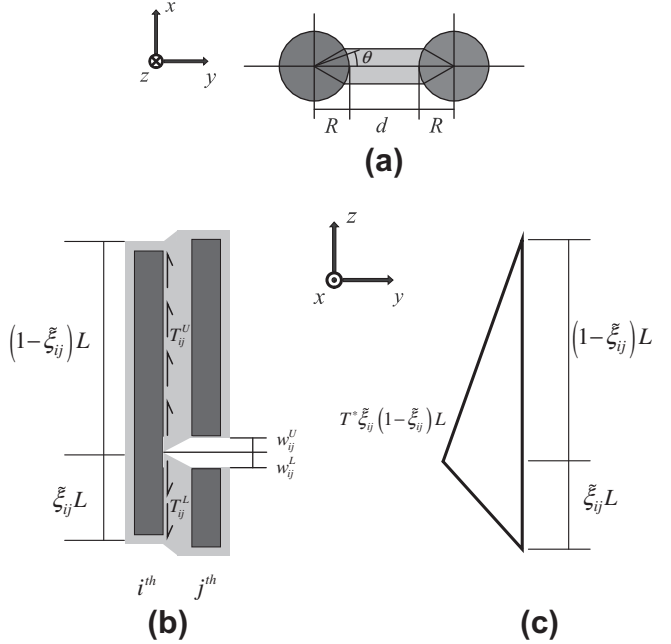


Fig. 4. Schematic of a pair of neighboring fibers for theoretical analysis: (a) cross section view, (b) side view, (c) normal stress of the  $i$ th fiber generated by the shear stress between this pair.

### 2.1.1. Principle of minimum complementary energy

To obtain the stress and strain field of the composite, the principle of minimum complementary energy is used. The force equilibrium of the  $i$ th fiber asks

$$\sum_{j \in nb\_set_i} [T_{ij}^L \tilde{\xi}_{ij} - T_{ij}^U (1 - \tilde{\xi}_{ij})] = 0 \quad (8)$$

where  $nb\_set_i$  represents the neighboring fiber set of the  $i$ th fiber,  $T_{ij}^L$  and  $T_{ij}^U$  are the shear forces from the lower and upper parts of the  $j$ th fiber, respectively. A guessed stress field that satisfies the above equilibrium equation can be written as

$$\begin{Bmatrix} T_{ij}^L \\ T_{ij}^U \end{Bmatrix} = T^* \begin{Bmatrix} 1 - \tilde{\xi}_{ij} \\ \tilde{\xi}_{ij} \end{Bmatrix}, \quad (9)$$

where  $T^*$  is a parameter to be determined, and  $T_{ij}^L$  and  $T_{ij}^U$  are shown in Fig. 4b. The normal stress of the  $i$ th fiber generated by the shear stress from the  $j$ th fiber fibers is

$$\sigma_i^{(j)}(\tilde{z}) \pi R^2 = \begin{cases} T_{ij}^L \tilde{z} & \tilde{z} < \tilde{\xi}_{ij}L \\ T_{ij}^U (L - \tilde{z}) & \tilde{z} \geq \tilde{\xi}_{ij}L \end{cases} \quad (10)$$

and its distribution is shown as Fig. 4c. We can then use Eqs. (9) and (10) to express the total normal stress of the  $i$ th fiber as

$$\sigma_i(\tilde{z}) = \frac{T^*}{\pi R^2} \sum_{j \in nb\_set_i} [(1 - \tilde{\xi}_{ij}) \tilde{z} - \langle \tilde{z} - \tilde{\xi}_{ij}L \rangle] \quad (11)$$

where the function  $\langle \cdot \rangle$  represents the following operation:

$$\langle x \rangle = \begin{cases} 0 & x < 0 \\ x & x \geq 0 \end{cases} \quad (12)$$

Thus, the total strain energy of all fibers in the unit cell is:

$$\sum_{i=1}^s \pi R^2 \int_0^L \frac{\sigma_i^2(\tilde{z})}{2E_f} d\tilde{z} = \frac{s \kappa_1 L^3 (T^*)^2}{2\pi R^2 E_f} \quad (13)$$

where

$$\kappa_1 = \frac{1}{s} \sum_{i=1}^s \int_0^1 \left\{ \sum_{j \in nb\_set_i} \left\{ \left[ (1 - \tilde{\xi}_{ij})\tilde{\xi} - \langle \tilde{\xi} - \tilde{\xi}_{ij} \rangle \right] \right\}^2 d\tilde{\xi} \right\} \quad (14)$$

is a dimensionless factor depending only on the distribution of the fibers.

On the other hand, the strain energy of the matrix in the unit cell is

$$\frac{1}{2} \sum_{i=1}^s \sum_{j \in nb\_set_i} \int_0^L \int_{-\frac{R}{2}}^{\frac{R}{2}} \frac{[\tau_{ij}(\theta)]^2}{2G_m} (d + 2R - 2R\cos\theta) dx dz = \frac{s\beta_2 L(T^*)^2}{8C_0 G_m} \quad (15)$$

where

$$\beta_2 = \frac{2}{s} \sum_{i=1}^s \left[ \sum_{j \in nb\_set_i} \tilde{\xi}_{ij}(1 - \tilde{\xi}_{ij}) \right] \quad (16)$$

is also a dimensionless factor depending only on the distribution of the fibers. Thus, the complementary energy in the unit cell is:

$$\Pi_C = s \left[ \frac{\kappa_1 L^3}{2\pi R^2 E_f} + \frac{\beta_2 L}{8C_0 G_m} \right] (T^*)^2 - s\bar{F}\Delta \quad (17)$$

where  $\Delta$  is the longitudinal extension of the unit cell and

$$\bar{F} = \frac{1}{s} \sum_{i=1}^s \sum_{j \in nb\_set_i} \left[ \frac{1}{2} T_{ij}^U (1 - \tilde{\xi}_{ij})^2 L + \frac{1}{2} T_{ij}^L \tilde{z}_j^2 L \right] = \frac{1}{4} \beta_2 T^* L \quad (18)$$

is the average external force imposed on a single fiber which can be derived from Fig. 4c. According to the principle of minimum complementary energy, let  $\frac{d\Pi_C}{dT^*}$  equal to zero, then we can solve  $T^*$  as

$$T^* = \frac{\Delta}{\frac{4\kappa_1 L^2}{\beta_2 \pi R^2 E_f} + \frac{1}{C_0 G_m}} \quad (19)$$

Once  $T^*$  is determined, all stresses and strains are known, and we can then compute the effective mechanical properties of fiber-reinforced composites.

### 2.1.2. Prediction of effective longitudinal modulus

Since it is assumed that the tensile loading is mainly sustained by fibers, according to Eq. (18), the effective normal stress of the composites is

$$\sigma_{eff} = \Phi \frac{\bar{F}}{\pi R^2} = \frac{\Phi \beta_2 T^* L}{4\pi R^2} \quad (20)$$

Substituting Eq. (19) into the above equation gives

$$\sigma_{eff} = \frac{1}{\frac{1}{\beta_1 \Phi E_f} + \frac{\pi}{\beta_2 \rho^2 \Phi C_0 G_m}} \frac{\Delta}{L} \quad (21)$$

where

$$\beta_1 = \frac{\beta_2^2}{16\kappa_1} = \frac{\left[ \sum_{i=1}^s \sum_{j \in nb\_set_i} \tilde{\xi}_{ij}(1 - \tilde{\xi}_{ij}) \right]^2}{4s \sum_{i=1}^s \int_0^1 \left\{ \sum_{j \in nb\_set_i} [(1 - \tilde{\xi}_{ij})\tilde{\xi} - \langle \tilde{\xi} - \tilde{\xi}_{ij} \rangle] \right\}^2 d\tilde{\xi}} \quad (22)$$

As the effective strain of the composite is  $\varepsilon_{eff} = \Delta/L$ , the effective longitudinal modulus of the composite is

$$E_{eff} = \frac{\sigma_{eff}}{\varepsilon_{eff}} = \frac{1}{\frac{1}{\beta_1 \Phi E_f} + \frac{\pi}{\beta_2 \rho^2 \Phi C_0 G_m}} \quad (23)$$

It should be pointed out that the predicted modulus derived from principle of minimum complementary energy should be the lower bound of the true value.

### 2.1.3. Prediction of longitudinal strength

The longitudinal strength is reached when the maximum shear stress in the matrix reaches the shear strength of the matrix  $\tau_m^c$  or the maximum normal stress on the fibers reaches the tension strength  $\sigma_f^c$  of the fibers.

If shear failure happens in the matrix, according to Eqs. (7) and (9), we can get

$$\tau_m^c = \frac{\kappa_2 T^*}{C_0 d} \quad (24)$$

where

$$\kappa_2 = \max_{i,j \in nb\_set_i} \{ \tilde{\xi}_{ij}, 1 - \tilde{\xi}_{ij} \} \quad (25)$$

is a dimensionless factor depending only on the distribution of the fibers. The corresponding critical effective stress  $\sigma_{eff}^{c,\tau}$  can be computed from Eqs. (24) and (20) as

$$\sigma_{eff}^{c,\tau} = \frac{\Phi \beta_2 \rho C_0 d \tau_m^c}{2\pi R \kappa_2} \quad (26)$$

If a tension failure happens in the fibers, according to Eq. (11), we can get

$$\sigma_f^c = \max_i \max_{\tilde{z}} \sigma_i(\tilde{z}) = \frac{\kappa_3 T^* L}{\pi R^2} \quad (27)$$

where

$$\kappa_3 = \max_i \max_{k \in nb\_set_i} \left\{ \sum_{j \in nb\_set_i} \left[ (1 - \tilde{\xi}_{ij})\tilde{\xi}_{ik} - \langle \tilde{\xi}_{ik} - \tilde{\xi}_{ij} \rangle \right] \right\} \quad (28)$$

is a dimensionless factor depending only on the distribution of the fibers. The corresponding critical effective stress  $\sigma_{eff}^{c,\sigma}$  can be computed from Eqs. (27) and (20) as

$$\sigma_{eff}^{c,\sigma} = \frac{\Phi \beta_2 \sigma_f^c}{4\kappa_3} \quad (29)$$

Obviously, shear failure in the matrix happens if  $\sigma_{eff}^{c,\tau} < \sigma_{eff}^{c,\sigma}$ , while tension failure in the fibers happens if  $\sigma_{eff}^{c,\tau} > \sigma_{eff}^{c,\sigma}$ . Based on Eqs. 16, 25, 26, 28, and 29, the effective longitudinal strength of the composites is

$$\sigma_{eff}^c = \begin{cases} \Phi \tau_m^c \left( \frac{C_0 d}{R} \right)^{\frac{1}{\beta_4}} \rho, & \rho \leq \rho^c \\ \Phi \sigma_f^c \frac{1}{\beta_3}, & \rho > \rho^c \end{cases} \quad (30)$$

where

$$\rho^c = \frac{\beta_4 \sigma_f^c}{\beta_3 \tau_m^c} \frac{R}{C_0 d} \quad (31)$$

is the critical aspect ratio that separates matrix failure ( $\rho \leq \rho^c$ ) from fiber failure ( $\rho \geq \rho^c$ ), and  $\beta_3$  and  $\beta_4$  are two non-dimensional factors representing the effect of non-uniform distribution of fibers on the strength of the composite, and are given by

$$\beta_3 = \frac{4\kappa_3}{\beta_2} = \frac{2s \max_{k \in nb\_set_i} \left\{ \sum_{j \in nb\_set_i} \left[ (1 - \tilde{\xi}_{ij})\tilde{\xi}_{ik} - \langle \tilde{\xi}_{ik} - \tilde{\xi}_{ij} \rangle \right] \right\}}{\sum_{i=1}^s \left[ \sum_{j \in nb\_set_i} \tilde{\xi}_{ij} (1 - \tilde{\xi}_{ij}) \right]}, \quad (32)$$

$$\beta_4 = \frac{2\pi \kappa_2}{\beta_2} = \frac{\pi s \max_{j \in nb\_set_i} \{ \tilde{\xi}_{ij}, 1 - \tilde{\xi}_{ij} \}}{\sum_{i=1}^s \left[ \sum_{j \in nb\_set_i} \tilde{\xi}_{ij} (1 - \tilde{\xi}_{ij}) \right]}. \quad (33)$$

Based on Eq. (30), when  $\rho < \rho^c$ , a shear failure happens in the matrix and the failure strength has a linear relationship with the aspect ratio of fibers. When  $\rho \geq \rho^c$ , tension failure happens in the fibers and the ultimate strength does not increase with increasing the aspect ratio anymore.

The failure strain and energy storage capacity can also be determined as  $\varepsilon_{eff}^c = \sigma_{eff}^c/E_{eff}$  and  $w_{eff}^c = (\sigma_{eff}^c)^2/(2E_{eff})$ , respectively. Together with Eqs. (23) and (30), the proposed 3D tension-shear chain model gives the estimates of effective modulus, strength, failure strain and energy storage capacity of unidirectional short fiber reinforced composites with various distributions.

Although there are infinite distributions of fibers, all the information about distribution can be incorporated into two dimensionless factors  $\beta_1$  and  $\beta_2$  when determining the modulus of composites. Similarly, there are another two dimensionless factors  $\beta_3$  and  $\beta_4$  only related to the distribution in determining the strength of composites. Thus, we name  $\beta_1, \beta_2$  as stiffness distribution factors and  $\beta_3, \beta_4$  as strength distribution factors. For any distribution  $(\xi_1, \xi_2, \dots, \xi_s)$ , they can be computed through Eqs. 1, 16, 22, 32, and 33. For long fibers ( $\rho > \rho^c$ ),  $\beta_1$  and  $\beta_3$  play major roles, smaller values imply higher stiffness and strength. For relatively short fiber ( $\rho < \rho^c$ ),  $\beta_2$  and  $\beta_4$  have more significant influence, still smaller values correspond to higher stiffness and strength.

The introduction of stiffness and strength distribution factors greatly simplifies the comparison of corresponding mechanical properties among different distributions. It also facilitates engineers and technicians on evaluating the mechanical properties of short fiber reinforced composites. Moreover, the equations also reveal the effect of physical properties and geometric parameters of the constituents on the mechanical properties of composite. This provides a theoretical guidance to the design of short fiber reinforced composites.

## 2.2. FEM model

In order to verify the 3D tension-shear chain model, we also used ABAQUS to establish FEM models of the unit cell with different fibers distributions. The mesh is shown in Fig. 5, in which C3D8R element is used for the simulations. The cell geometry in FEM varies for different simulated samples to make sure they are directly comparable. By keeping  $R$  fixed to be constant (unit length),  $d$  is determined as to match the volume fraction of fibers, and  $l$  can be determined by the fiber aspect ratio. The longitudinal gap between neighboring fibers is set to be around one unit length, so that it is at least one order in magnitude less than the length of fibers. Periodic boundary conditions are imposed on the six surface of the unit cell and a tension load is exerted along the direction of fibers.

## 3. The effects of parameters on the mechanical properties of composites

### 3.1. Strength of composite with different fibers distribution

The gaps between fibers within “stairwise staggering” distribute in a stairwise pattern (Fig. 6a and b), which is observed in some biocomposites such as bones (see the 3D pattern in Fig. 1b). In this case, relative positions of neighboring fibers for every fiber are the same, and  $\tilde{\xi}_{ij} = \{0, (n-1)/n, (n-1)/n, 0, 1/n, 1/n\}$  for the  $i$ th fiber. We can compute the strength distribution factors as  $\beta_3 = n/(n-1)$ ,  $\beta_4 = n\pi/4$ . When  $n = 2$ , the longitudinal gap is just located at the center of neighboring fibers, and the pattern is called “regular staggering” hereafter. Substituting these distribution factors into Eq. (30) gives the strength for the composites with stairwise staggering,

$$\sigma_{eff}^c = \begin{cases} \Phi \tau_m^c \left( \frac{C_0 d}{R} \right) \frac{4}{nn} \rho, & \rho \leq \rho^c \\ \Phi \sigma_f^c \frac{n-1}{n}, & \rho > \rho^c \end{cases} \quad (34)$$

where

$$\rho^c = \frac{\pi(n-1)}{4} \frac{\sigma_f^c}{\tau_m^c} \frac{R}{C_0 d}. \quad (35)$$

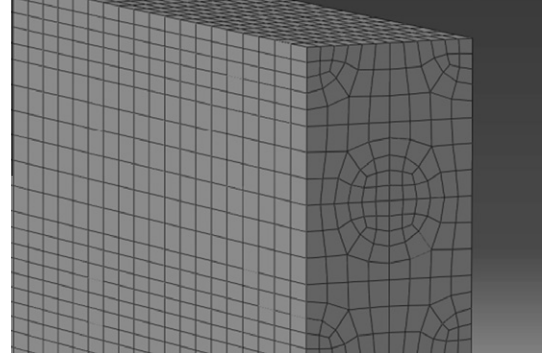


Fig. 5. Mesh of the FEM model.

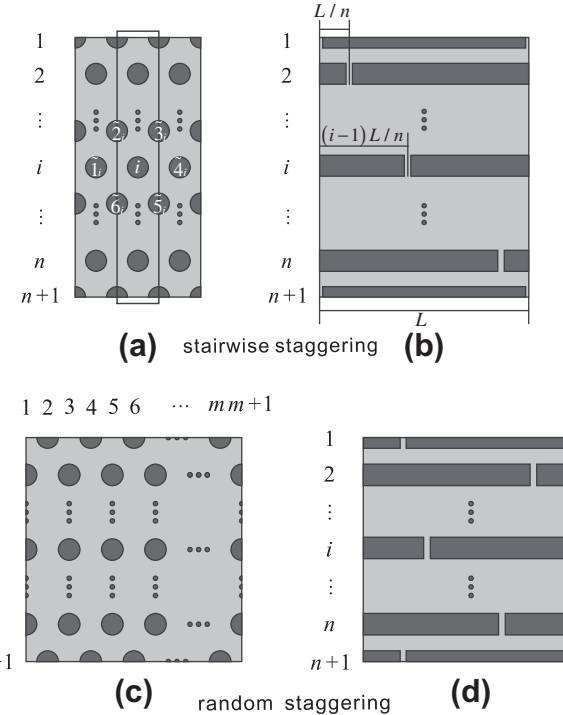
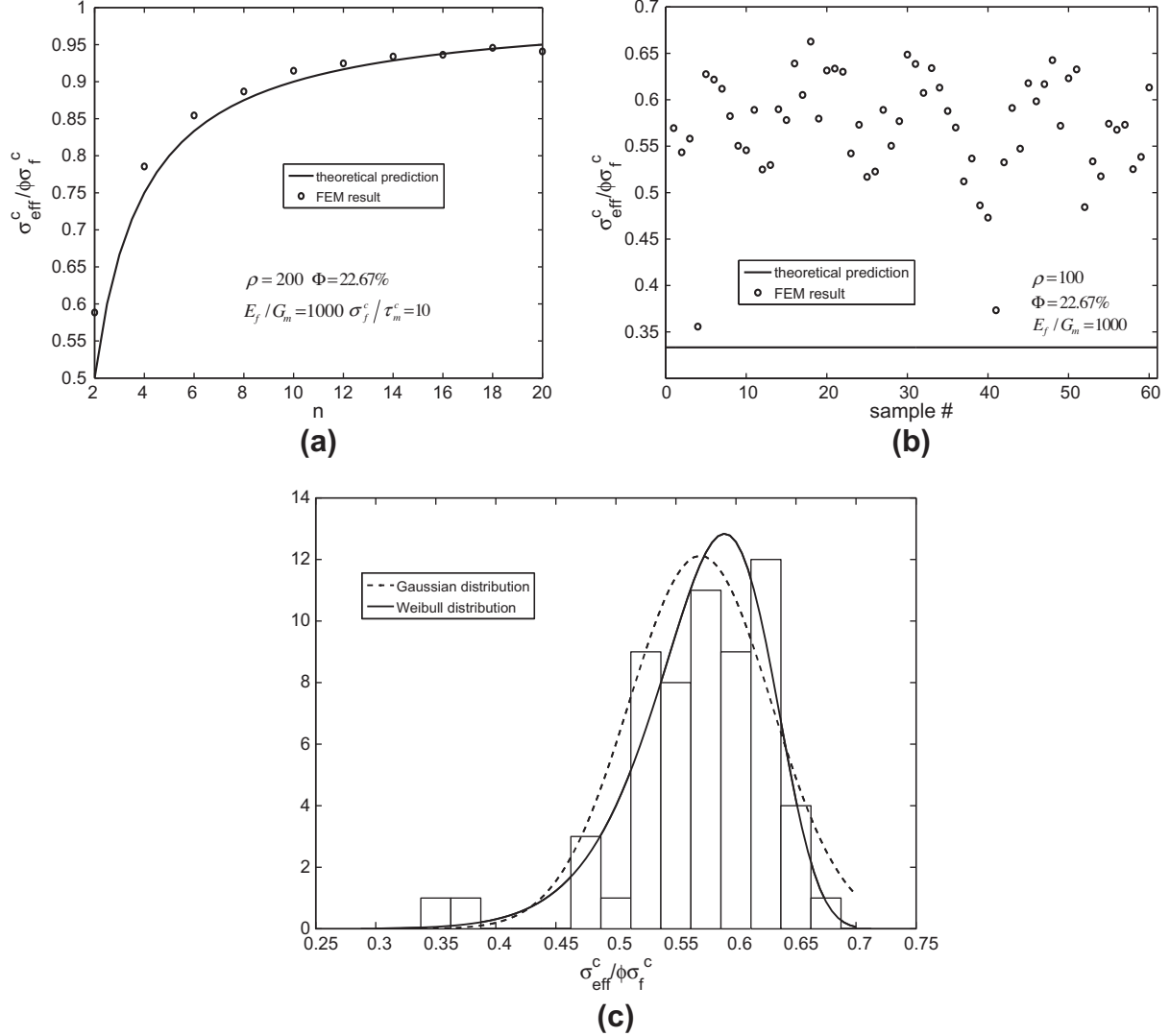


Fig. 6. Unit cell of the composite with (a), (b) stairwise staggering and (c), (d) random staggering.

Fig. 7a shows the predicted and simulated the normalized strength  $\sigma_{eff}^c/\Phi\sigma_f^c$  versus the periodic number  $n$  for composites with stairwise staggering, with a set of parameters  $\rho = 200$ ,  $\sigma_f^c/\tau_m^c = 10$ ,  $\Phi = 22.67\%$  and  $E_f/G_m = 1000$ . We can see that the predicted composite strength is in good agreement with the FEM results. The figure also shows that, provided a large aspect ratio of fiber ( $\rho = 200$  compared to  $\rho^c = 155$  at  $n = 20$  here), the strength increases with the periodic number  $n$ , and gradually approaches the strength of continuous fiber reinforced composite  $\Phi\sigma_f^c$  when  $n$  is sufficiently large, as indicated by Eq. (34) at  $\rho > \rho^c$ . This provides a possible explanation why some biocomposites adopt such patterns and also inspires us to improve the strength of biomimetic materials by increasing the periodic number.

As mentioned in Section 1, random distribution of reinforcements is most likely to occur in practical fabrications. For studies on the randomness nature of both the distribution and the strength of discontinuous-fibers, Phoenix and coworkers have built up a general framework of statistical model through a series of pioneering works (e.g., [31–32]). Here we study the random distribution



**Fig. 7.** Theoretical prediction and FEM results of strength for composites with different distribution: (a) stairwise staggering, (b), (c) random staggering.

case under the assumptions and constraints described in Section 2.1, say all fibers are with identical length, diameter, strength, longitudinal and lateral spacing to their neighbors. In another word, only  $\xi_i$  (or  $\xi_j$ , say the longitudinal position of short-fiber end) are random variables, and consequently so are  $\xi_{ij}$  ( $j \in nb\_set_i$ ). For simplicity, all  $\xi_i$  ( $\xi_j$ ) are assumed independent and uniformly distributed between 0 and 1, and consequently so are  $\xi_{ij}$  ( $j \in nb\_set_i$ ) for the  $i$ th fiber. Then, the average values of  $\kappa_1$  and  $\beta_2$  in Eqs. (14) and (16) can be calculated to be  $\frac{19}{60}$  and 2 respectively. Note that the average values are independent of the size of unit cell  $s$ , which is understandable from the view point of probability and statistics. With varying  $\xi_{ij}$  ( $j \in nb\_set_i$ ) from 0 to 1, the maximums,  $\kappa_2 = 1$  at  $\xi_{ij} = 0$  or 1 ( $j \in nb\_set_i$ ) and  $\kappa_3 = \frac{3}{2}$  at  $\xi_{ij} = \xi_{ik} = \frac{1}{2}$  ( $j, k \in nb\_set_i$ ), which corresponds to the worst situation for fiber and nearby matrix. Therefore, the strength distribution factors for random staggering distribution can be calculated to be  $\beta_3 = \frac{4\kappa_3}{\beta_2} = 3$  and  $\beta_4 = \frac{2\pi\kappa_3}{\beta_2} = \pi$ . Substituting these distribution factors in Eq. (30) gives a lower-bound strength evaluation of the random staggering

$$\sigma_{eff}^c = \begin{cases} \Phi\tau_m^c \frac{C_0 d}{R} \frac{1}{\pi} \rho, & \rho \leq \rho^c \\ \Phi\sigma_f^c \cdot \frac{1}{3}, & \rho > \rho^c \end{cases} \quad (36)$$

where

$$\rho^c = \frac{\pi}{3} \frac{\sigma_f^c}{\tau_m^c} \frac{R}{C_0 d}. \quad (37)$$

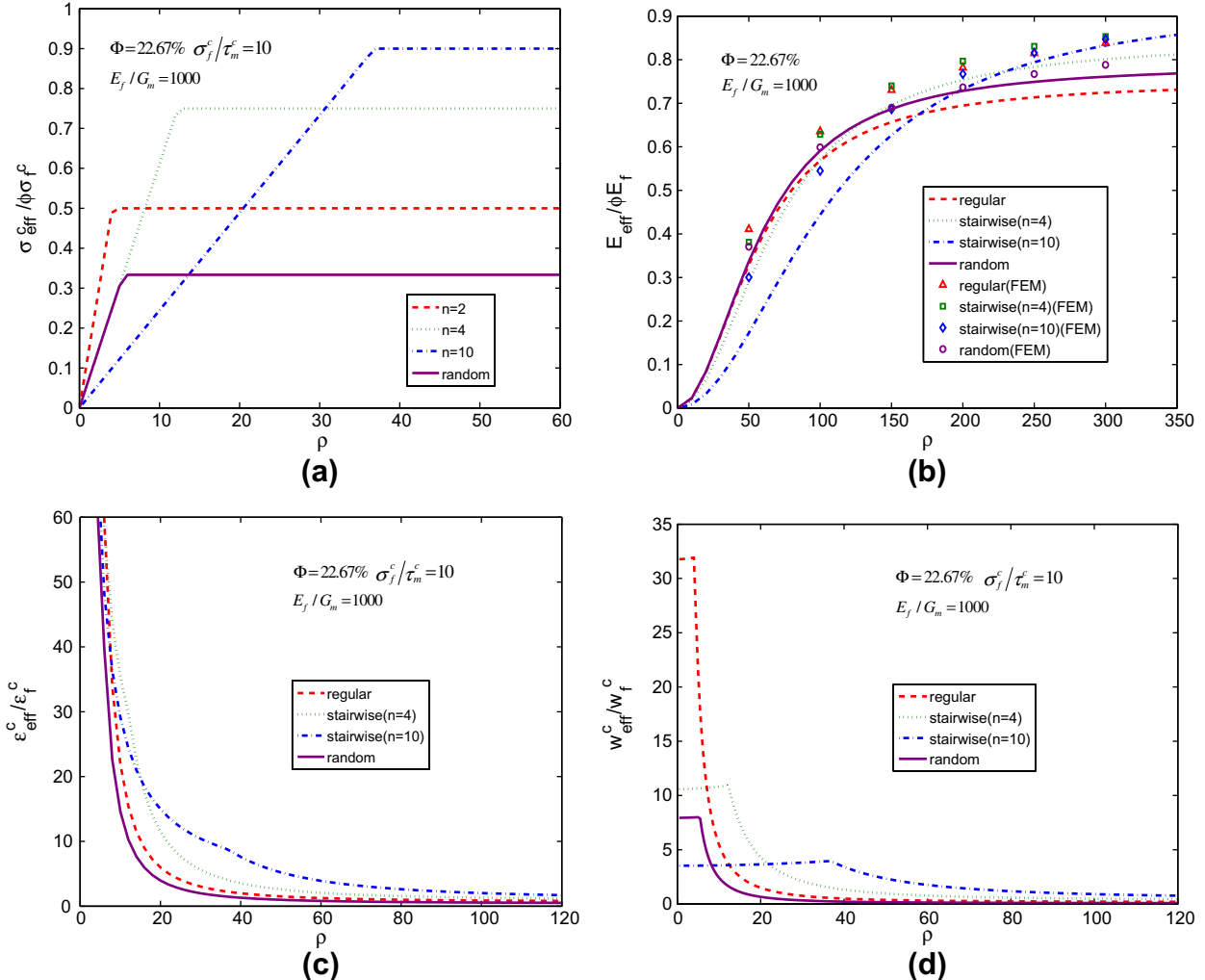
According to Monte Carlo method, Fig. 7b shows normalized simulated strengths of 60 samples of the random staggering composite with fiber lattice  $m \times n = 12 \times 12$ . Limited by the capability of personal computer, the unit cell used to calculate the strength cannot be large enough. However, a number of random samples of Monte Carlo simulations can compromise the limitation and make an outline portrait of the strength of random staggering. From Fig. 7b, it can be seen that the calculated sample strengths are always above the theoretical prediction, but there are also a very few samples quite close to the predicted strength. Noting that the predicted strength by our 3D tension-shear chain model (the line in Fig. 7b) corresponds to the worst case, the theoretical prediction is well verified by the FEM simulations. The statistical chart of the sample data has been plotted in Fig. 7c, which fits better to the well-known Weibull probability distribution.

Fig. 8a shows the normalized strength  $\sigma_{eff}^c / \Phi\sigma_f^c$  of short fiber reinforced composite varying with the fiber aspect ratio  $\rho$  for dif-

ferent distributions. The parameters are taken as  $\sigma_f^c/\tau_m^c = 10$ ,  $\Phi = 22.67\%$  and  $E_f/G_m = 1000$ . For each distribution, the strength first increases as the fiber aspect ratio increases (matrix failure regime, indicated by Eqs. (34) and (36) at  $(\rho \leq \rho^c)$ ), and then reaches a roof when the critical aspect ratio is reached and beyond (fiber failure regime, indicated by Eqs. (34) and (36) at  $\rho > \rho^c$ ). Comparing the different distributions, it is found that for very short fibers, i.e., in the region of just matrix failure, the stairwise staggering with smaller periodic number  $n$  has larger strength, which should be attributed to its higher inclination of strength with respect to the fiber aspect ratio as suggested by Eq. (34) at  $(\rho \leq \rho^c)$ . For very large fiber aspect ratio, or say in the region of only fiber failure, larger periodic number  $n$  leads to higher strength, which is understandable according to Eq. (34) at  $\rho > \rho^c$ . It is also worth noting that the strength of composite with random staggering is generally far lower than that with controlled distributions. This suggests that there is still a large space for material scientists and engineers to improve the performances of biomimetic composites via more strictly controlling the distribution of reinforcements.

### 3.2. Effective modulus of composites with different fiber distributions

As in the case of stairwise staggering distribution, for the  $i$ th fiber  $\xi_{ij} = \{0, (n-1)/n, (n-1)/n, 0, 1/n, 1/n\}$ , we can then compute the stiffness distribution factors from Eqs. (22) and (16) as



**Fig. 8.** Comparison of (a) strength, (b) Young's modulus, (c) failure strain, and (d) energy storage capacity for composites with different distributions.

$\beta_1 = 3(n-1)^2/[n(3n-4)]$ ,  $\beta_2 = 8(n-1)/n^2$ . Substituting them in Eq. (23) gives the predicted modulus for stairwise staggering distribution,

$$E_{eff} = \frac{1}{\frac{n(3n-4)}{3(n-1)^2\Phi E_f} + \frac{n^2\pi}{8(n-1)\rho^2\Phi C_0 G_m}}. \quad (38)$$

Regarding “random staggering” (Fig. 6c and d) widely seen in biological and biomimetic materials, the average values of the stiffness distribution factors for random staggering distribution can be calculated as stated in the last subsection,  $\beta_1 = \frac{\beta_2^2}{16K_1} = 15/19$  and  $\beta_2 = 2$ . Substituting these factors in Eq. (23) yields the average modulus for the random staggering

$$E_{eff} = \frac{1}{\frac{19}{15\Phi E_f} + \frac{\pi}{2\rho^2\Phi C_0 G_m}} \quad (39)$$

Fig. 8b shows the predicted and simulated normalized stiffness  $E_{eff}/\Phi E_f$  versus the fiber aspect ratio  $\rho$  for the composites with regular staggering ( $n = 2$ ), stairwise staggering ( $n = 4$  and  $n = 10$ ) and random staggering. The simulated modulus for the random staggering distribution is an average of a large number of calculated samples ( $m \times n = 12 \times 12$ ). The number of calculated samples is justified large enough; in another word, there is no evident change found in the average modulus even with more samples included. It can be seen that the predicted values of modulus basically agree

with the simulated data. However, the predicted stiffness is a little bit smaller than the FEM results when the fiber aspect ratio is low. This is because we do not account for the tensile stiffness of the matrix, which become more significant when the fiber aspect ratio diminishes. As the plots show, the fiber distribution does have significant influence on the stiffness of composites, and the effective modulus of short fiber reinforced composites increases with the increase of the aspect ratio. It is also noted that the stiffness of composites with random staggering is comparable to that with other regular distributions.

### 3.3. Failure strain of composite with different fiber distributions

We have verified the performance of 3D tension-shear chain model in estimating the stiffness and strength of short fiber reinforced composite in the above discussions. Furthermore, Fig. 8c shows the effect of different distributions on the failure strain ( $\epsilon_{eff}^c = \sigma_{eff}^c/E_{eff}$ ) of short fiber reinforced composite. As we can see, different with the stiffness and the strength, the failure strain of staggering distribution decreases as the aspect ratio increases. It is understandable since the strength fast reaches a plateau with increasing the aspect ratio of fibers while the effective Young's modulus always increases. The decrease of failure strain against fiber aspect ratio is fastest for random staggering, and becomes slightly slower as the periodic number increases for stairwise staggering (including regular staggering  $n = 2$ ).

### 3.4. Energy storage capacity of composite with different fiber distributions

In order to evaluate the overall mechanical properties of short fiber reinforced composites, Fig. 8d demonstrates the effect of different distributions on the energy storage capacity of composites,  $w_{eff}^c = (\sigma_{eff}^c)^2/(2E_{eff})$ , which well combines effective strength and failure strain. It is found that the highest energy storage capacity for each distribution appears at the critical aspect ratio. Generally, the stairwise staggering with a smaller periodic number has a larger peak value of the energy storage capacity. The peak value for regular staggering is several times or even one order larger than that of the other distributions.

## 4. Conclusions

A three-dimensional tension-shear chain model for the unidirectional short fiber reinforced composites is developed in this paper, which can well depict the relationship between the fiber distributions and the effective mechanical properties like stiffness, strength, failure strain and energy storage capacity. FEM simulations have also been carried out to verify the accuracy of the model. The following conclusions can be drawn.

First of all, besides the volume fraction, shape and orientation of the reinforcements, the distribution of fibers also plays a significant role in the mechanical properties of unidirectional composites. Four distribution factors, the stiffness distribution factors  $\beta_1$ ,  $\beta_2$  and the strength distribution factors  $\beta_3$  and  $\beta_4$ , are identified to completely characterize the influence of the reinforcement distribution, and they can be easily computed. It should be emphasized that classical homogenization-based mesomechanical approaches, such as the Mori-Tanaka method, cannot take this distribution effect into account.

Secondly, it is found that stairwise staggering (including regular staggering with  $n = 2$ ), which is adopted by the nature, could achieve overall excellent performance, namely high stiffness and strength comparable to those of the reinforcing fibers as well as large failure strain and energy storage capacity comparable to those

of the soft matrix. The performance of random staggering is obviously lower than stairwise staggering, which indicates that precisely controlled microstructure is an efficient way to further improve performance of biomimetic and other man-made composites.

In a word, our proposed 3D tension-shear chain model well characterizing the relationship of mechanical properties and fiber alignments may provide useful guidelines for the design of high performance short fiber reinforced composites, e.g. carbon nanotube composites.

## Acknowledgements

The authors are grateful for the support from National Natural Science Foundation of China (Grant Nos. 10732050, 90816006, 11090334, and 10820101048), and National Basic Research Program of China (973 Program) Grant Nos. 2007CB936803 and 2010CB832701. ZZ also thanks the support from the A\*Star Visiting Investigator Program "Size Effects in Small Scale Materials" hosted at the Institute of High Performance Computing in Singapore.

## References

- [1] Jackson AP, Vincent JFV, Turner RM. The mechanical design of nacre. Proc Royal Soc London. Series B, Biol Sci 1988;234:415–40.
- [2] Currey JD. Mechanical properties of mother of pearl in tension. Proc Royal Soc London. Series B 1977;196:443–63.
- [3] Kamat S, Su X, Ballarini R, et al. Structural basis for the fracture toughness of the shell of the conch Strombusigas. Nature 2000;405:1036.
- [4] Landis WJ. The strength of a calcified tissue depends in part on the molecular structure and organization of its constituent mineral crystals in their organic matrix. Bone 1995;16:533–44.
- [5] Menig R, Meyers MH, Meyers MA, et al. Quasi-static and dynamic mechanical response of *Haliotis rufescens* (abalone) shells. Acta Mater. 2000;48:2383–98.
- [6] Landis WJ, Hodgens KJ, Song MJ, et al. Mineralization of collagen may occur on fibril surfaces: evidence from conventional and high-voltage electron microscopy and three-dimensional imaging. J Struct Biol 1996;117:24–35.
- [7] Roschger P, Grabner BM, Rinnerthaler S, et al. Structural development of the mineralized tissue in the human L4 vertebral body. J Struct Biol 2001;136:126–36.
- [8] Rho J-Y, Kuhn-Spearing L, Ziopoulos P. Mechanical properties and the hierarchical structure of bone. Med Eng Phys 1998;20:92–102.
- [9] Gao H, Ji B, Jager IL, et al. Materials become insensitive to flaws at nanoscale: lessons from nature. Proc National Acad Sci USA 2003;100:5597–600.
- [10] Liu B, Zhang L, Gao H. Poisson ratio can play a crucial role in mechanical properties of biocomposites. Mech Mater 2006;38:1128–42.
- [11] Jager I, Fratzl P. Mineralized collagen fibrils: a mechanical model with a staggered arrangement of mineral particles. Biophys J 2000;79:1737.
- [12] Ji B, Gao H. Mechanical properties of nanostructure of biological materials. J Mech Phys Solids 2004;52:1963–90.
- [13] Tang Z, Kotov NA, Magonov S, et al. Nanostructured artificial nacre. Nat Mater 2003;2:413–8.
- [14] Bonderer LJ, Studart AR, Gauckler LJ. Bioinspired design and assembly of platelet reinforced polymer films. Science 2008;319:1069–73.
- [15] Zhang ZQ, Liu B, Huang Y, et al. Mechanical properties of unidirectional nanocomposites with non-uniformly or randomly staggered platelet distribution. J Mech Phys Solids 2010;58:1646–60.
- [16] Van Hattum FWJ, Bernardo CA. A model to predict the strength of short fiber composites. Polym Compos 1999;20:524–33.
- [17] Laranjeira E, et al. Influence of fiber orientation on the mechanical properties of polyester/jute composites. J Reinf Plast Compos 2006;25:1269–2378.
- [18] Zhu YT, Zong GS. On the application of the statistical strength model of fiber reinforced composites. J Compos Mater 1993;27:944–59.
- [19] Berthelot JM, Cupic A, Brou KA. Stress distribution and effective longitudinal Young's modulus of unidirectional short fibre composites. J Compos Mater 1993;27:1391–425.
- [20] Qian D, Dickey EC, Andrews R, et al. Load transfer and deformation mechanisms in carbon nanotube-polystyrene composites. Appl Phys Lett 2000;76:2868–70.
- [21] Ajayan PM, Tour JM. Materials science – nanotube composites. Nature 2007;447(7148):1066–8.
- [22] Thostenson ET, Ren ZF, Chou TW. Advances in the science and technology of carbon nanotubes and their composites: a review. Compos Sci Technol 2001;61(13):1899–912.
- [23] Jia ZJ. The research of carbon nanotube/polymer composite materials. Beijing: Tsinghua University; 1999.
- [24] Shi DL. The mechanical properties of carbon nanotubes and their composites. Beijing: Tsinghua University; 2005.

- [25] Gao GH, Cagin T, Goddard WA. Energetics, structure, mechanical and vibrational properties of single-walled carbon nanotubes. *Nanotechnology* 1998;9:184–91.
- [26] Jin L, Bower C, Zhou O. Alignment of carbon nanotubes in a polymer matrix by mechanical stretching. *Appl Phys Lett* 1998;73:1197–9.
- [27] Haggenmueller R, Gommans HH, Rinzler AG, et al. Aligned single-wall carbon nanotubes in composites by melt processing methods. *Chem Phys Lett* 2000;330:219–25.
- [28] Bower C, Rosen R, Jin L, et al. Deformation of carbon nanotubes in nanotube-polymer composites. *Appl Phys Lett* 1999;74:3317–9.
- [29] Jin Z, Pramoda KP, Xu G, et al. Dynamic mechanical behavior of melt-processed multi-walled carbon nanotube/poly(methyl methacrylate) composites. *Chem Phys Lett* 2001;337:43–7.
- [30] Zhang ZQ, Liu B. The prediction of axial equivalent modulus for composites reinforced by staggered alignment discontinuous fibers. *Eng Mech* 2010;2: 235–40.
- [31] Ibnabdeljalil M, Phoenix SL. Scalings in the statistical failure of brittle matrix composites with discontinuous fibers: analysis and Monte Carlo simulations. *Acta Metall Mater* 1995;43:2975–83.
- [32] Phoenix SL, Ibnabdeljalil M, Hui CY. Size effects in the distribution for strength of brittle matrix fibrous composites. *Int J Solids Struct* 1997;34: 545–68.
- [33] Liu G, Ji BH, Hwang KC, et al. Analytical solutions of the displacement and stress fields of the nanocomposite structure of biological materials. *Compos Sci Technol* 2011;71:1190–5.